Pergamon

PII: S0301-9322(96)00011-0

Int. J. Multiphase Flow Vol. 22, No. 4, pp. 713–732, 1996

0301-9322/96 $15.00 + 0.00

DESIGN OF A FLOW METERING PROCESS FOR TWO-PHASE DISPERSED FLOWS

C. BOYER and H. LEMONNIER

Commissariat à l'Energie Atomique—Grenoble, DRN/DTP/STI, Laboratoire d'Etudes Fondamentales, 17 Avenue des Martyrs, F 38054 Grenoble Cedex 9, France

(Received 15 December 1994; in revised form 8 February 1996)

Abstract—In this paper, we will describe the methodology used to conceive and size a flowmeter for two-phase dispersed flows. The Venturi having been chosen as the velocity measurement device, we focus on its measurement sensitivity to the velocity slip between the phases at the throat. Among the different two-phase flow models reviewed, an original one has been selected and adapted to predict; velocity and pressure distributions along a Venturi tube with air/water and oil/water flows. Bubble and liquid velocity calculations performed by this model are compared with experimental data to show a good agreement between predicted and measured velocities at the throat. The superiority of this model is shown by comparing its pressure drop predictions with those obtained with more classical two fluid models and available experimental data. Finally the influence of the bubble diameter on the pressure drop calculations and flow rate evaluations has been studied to determine the maximum admissible bubble diameter and then to size the mixer set upstream of the Venturi. Copyright © 1996 Elsevier Science Ltd.

Key Words: two-phase dispersed flows, multiphase flow metering, Venturi meter

1. INTRODUCTION

The accurate measurement of multiphase flows composed of oil, water, and gas phases is of great practical significance in many industries, such as chemical and process industries, power plants, oil refineries, and in particular, the exploration and production of crude oil and natural gas. The flow of crude oil, natural gas and water in a three-phase mixture flowing in an oil well constitutes a standard condition in oil production.

As reported by Delhaye (1989) and Hewitt *et al.* (1988), the main requirements for measuring flow rates are focused on four areas:

(1) Reservoir management,
(2) Custody transfer metering: here production from one field may be mixed with production from another with ownership of the two being different,
(3) Process control: when gas lift pumping or vapour injection is used, it is necessary to know the efficiency of the process, and
(4) Fiscal metering.

The accuracy expected for each flow rate measurement in the first three areas is about five percent of the measured value, whereas fiscal metering requires measurement with errors less than one percent. This last level of accuracy is obviously much more difficult to obtain. Among the available alternatives, there are three main possibilities of operation:

(1) To make all measurements when the flow is in its natural state (no perturbation),
(2) To homogenise the mixture to make all phase velocities equal, and
(3) To separate the phases and measure each individual phase using single phase techniques.

The second alternative, simpler than the first one (only one velocity to measure) and less intrusive than the last, appears to be a good compromise between complexity and accuracy as explained by Hewitt *et al.* (1988). It also opens the way to the application of a large variety of currently used well known techniques in single-phase flow, to two-phase gas–liquid flows in nuclear and chemical engineering. Choosing this method of operation, our multiphase flow meter will be naturally

composed of a mixer (upstream of the measurement section), a device to measure velocity and one or two devices to measure phase fractions.

Among the large variety of techniques to measure velocity which have been presented by Hewitt (1988), many neutron-based techniques, although very promising, seem to be unrealistic for submerged, ocean applications. Therefore, a simpler device, the Venturi meter has been chosen.

The main available techniques to determine phase fraction are: attenuation of X-rays or gamma rays (Delhaye *et al.* 1980), measurement of impedance (good results under laboratory conditions, but much more difficult to use in field situations), measurement of celerity or attenuation of ultrasonic waves. This last technique is very useful to measure void fraction and interfacial area in bubbly air–water flows (Bensler 1990). However, its extension to production, though promising, still needs much work.

To homogenise the flow upstream of the measurements, it is intended to utilise the static mixer OPTIMIX (Lecoffre *et al.* 1993). The fluids to be mixed cross two successive walls through holes with different diameters. In the first stage, the mixture is representative of the mean concentrations of the different species, and in the second, a finer mixing is obtained by creating a strong turbulent dissipation of energy. Using the model of Hinze and Kolmogorov (Hinze 1955; Sevik & Park 1973; Berne 1983), it is possible to predict the maximum droplet diameter from the dissipation rate. According to Lecoffre (1993), it is thus possible to size the mixer by an inverse calculation such that it generates a dispersion with a given maximum droplet diameter. This feature makes OPTIMIX quite attractive for our purpose.

Since we have been first interested in the choice of a device for determining the mean velocity, this paper emphasises the mean velocity measurement.

Widely used in single-phase and some two-phase measurements, the Venturi tube has the advantage of being easily designed and is not expensive. One of the most difficult problems that appears when used in two-phase flows is the velocity slip that occurs at the throat, making the interpretation of pressure drops ambiguous. It is therefore important to determine the maximum bubble diameter for which the velocity slip no longer influences the classical (homogeneous) flow rate evaluation.

In this paper we have first presented a review of the available two-phase dispersed flow models to predict pressure drops. Among them the model described by Kowe *et al.* (1988), based on the interstitial velocity approach, appears to be the most promising. This model is then adapted to predict air/water and oil/water flows. The superiority of this model is shown by comparing its predictions with those obtained with more classical two-fluid models and available data. Lastly, with this model it has been possible to predict the pressure drop for a range of bubble diameters, and thus to determine the optimal bubble or drop size required for a satisfactory operation of the meter.

2. STATE OF ART OF TWO-PHASE DISPERSED FLOW MODELS

The simplest model is the homogeneous flow model that can be derived from common international standards (BS 1042, ISO 1932). In this model, the flow rate is calculated using single-phase formulas and by replacing the density with the density of the two-phase mixture defined by:

$$\rho \equiv (1 - \epsilon)\rho_L + \epsilon\rho_G \qquad [1]$$

where ρ_L and ρ_G are the liquid and the gas densities, respectively, and ϵ is the void fraction. With this model (referred to as the HM hereafter), a single equation relates the pressure drop to the flow velocity and the void fraction.

Several authors have proposed correlations for predicting two-phase pressure drop in pipes, when the pressure drop of a single phase flow (in the same geometry), the quality, and the void fraction are known (Fairhust 1983; Chisholm 1983). These correlations provide a good estimate only when used within the range of parameters recommended by the authors, but, they rarely provide a satisfactory prediction when a change in operating variables occurs—a typical problem with empirical correlations.

Thang & Davis (1979) have determined the pressure distribution for a two-phase flow along Venturis by writing and solving mass balance equations for each phase and a momentum balance for the two-phase mixture. To close the model, these authors assumed that the relative velocity ratio u_G/u_L (u_G and u_L are the mean gas and liquid velocities, respectively) remains constant along the Venturi.

Several authors have proposed four-equation two-phase flow models to evaluate void fraction, phase velocity and pressure distributions (Winjgaarden & Biesheuvel 1984; Lewis & Davidson 1985; Kuo & Wallis 1988; Vromman 1988). The model presented by Lewis & Davidson (1985), referred to as the LDM hereafter, has been used as a reference two-fluid model for further comparison in this paper. It will be shortly described now. These authors considered a two-phase, one-dimensional, gas–liquid flow at steady state and used mass and momentum balances for each phase. The independent variables are u_L, u_G, ϵ and P, the area-averaged pressure common to both phases.

The mass balances have the classical form:

$$\frac{d}{dx}[A(1-\epsilon)u_L] = 0 \qquad [2]$$

$$\frac{d}{dx}[A\epsilon u_G] = 0 \qquad [3]$$

where A is the varying cross-sectional area of the Venturi and x is the abscissa along the Venturi axis. Owing to the large velocity range which is expected in our flow metering problem, the LDM has been simplified by assuming that both phases are incompressible.

The third LDM equation is the momentum balance for the gas phase. Its derivation is based on a force balance for a single bubble (inertial terms being negligible). This balance accounts for the added mass force, the pressure gradient force and a drag force, and results in:

$$V_b C_m \rho_L \left(u_G \frac{du_G}{dx} - u_L \frac{du_L}{dx} \right) + V_b \frac{dP}{dx} + \tau_d = 0 \qquad [4]$$

where V_b is the bubble volume, C_m is the added mass coefficient, τ_d is the drag force on the bubble, and P is the pressure. It is clear from [4] that bubble size must be given to close the problem.

The fourth and last equation of the LDM is a momentum balance for the mixture when the gas inertia is neglected:

$$(1-\epsilon)\rho_L u_L \frac{du_L}{dx} = -\frac{dP}{dx} - \rho_L g(1-\epsilon). \qquad [5]$$

As we will see further in this paper, the derivation of these two equations is not totally satisfactory and uncertainties may arise from the expression for the added mass force. By solving these equations one can predict the evolution of void fractions, velocities and pressures along the x-axis, provided that their upstream values are known.

Although he was primarily interested in critical flow rate modelling, Vromman (1988) uses the same basic equations but he expresses the force exerted by the liquid on the bubble with the results of Voinov (1973) and keeps a single term that describes the expansion of the bubble. In his model, the bubble radius r_b is no longer an input, but satisfies the interfacial area model of Hinze and Kolmogorov.

More recently Kowe *et al.* (1988) have proposed an original approach. Following the theoretical work of Cook & Harlow (1984), and the experiments reported by Bataille *et al.* (1990) to measure the volume of liquid driven by a bubble, they have regarded the two-phase media as consisting of three interacting fields (figure 1):

(1) The bubbles.
(2) The liquid displaced by the bubbles.
(3) The so-called 'interstitial liquid' that flows far away from bubbles.

As a result, Kowe *et al.* (1988) introduced a velocity field $\mathbf{u_0}$ for the interstitial liquid that differs from the mean liquid velocity field. According to these authors this velocity $\mathbf{u_0}$ is the velocity which should be used instead of the averaged liquid velocity in the closure laws when a reference velocity is required. This allows in particular the added mass force to be expressed in a more satisfactory manner.

As far as we have correctly understood their ideas, the volume of the fluid is partitioned in three domains each having its own velocity field. Letting V be the total volume occupied by the mixture:

(1) The bubbles occupy the volume ϵV and their velocity is $\mathbf{v}$.
(2) The liquid displaced by bubbles occupies the volume $C_m \epsilon V$ and flows with the same velocity as the bubbles $\mathbf{v}$.
(3) The interstitial liquid occupies the remaining volume $V - \epsilon V - C_m \epsilon V$ and flows with the velocity $\mathbf{u}_0$.

One of the reasons for sizing the displaced liquid volume with the added mass coefficient C_m originates from Darwin (1953) and is fully supported by the experiments of Bataille *et al.* (1990). These authors found that for bubble diameters between 2 and 4 mm the volume of liquid displaced by the motion of an isolated bubble in quiescent liquid, is exactly half the bubble volume.

In this three-field model approach the steady state mass balances become:

$$\frac{\mathrm{d}}{\mathrm{d}x}[A(1-\epsilon-C_m\epsilon)\mathbf{u}_0]+\frac{\mathrm{d}}{\mathrm{d}x}[AC_m\epsilon\mathbf{v}]=\mathbf{0} \qquad [6]$$

for the liquid, and

$$\frac{\mathrm{d}}{\mathrm{d}x}[A\epsilon\mathbf{v}]=\mathbf{0} \qquad [7]$$

for the dispersed phase.

Consistent to the three-field approach, it is necessary to introduce an interstitial pressure P_0 which is different from the mean pressure $\langle P \rangle$ obtained for the entire liquid. The difference between the two pressures is proportional to $(u_G - u_L)^2$ as already found by Prosperetti & Jones (1984) when they directly calculated the pressure force on the liquid containing bubbles.

In the three-field approach we have six unknowns: $\mathbf{u}_0$, $\langle \mathbf{u} \rangle$, $\mathbf{v}$, ϵ, P_0 and $\langle P \rangle$. In addition to the mass balances, the Kowe *et al.* (1988) model consists of two momentum balances and two equations derived from the added mass effects calculated by Voinov (1973). These two equations are independent from the already mentioned balance equations. These equations will be presented in the next section of this paper, as well as a discussion of the derivation of some terms.

3. EQUATIONS OF MOTION

3.1. Momentum balance for bubbles in liquid flow

To close the momentum balance we must provide the interfacial force exerted by the continuous phase on a bubble or a droplet (assumed to be spherical), in an unsteady flow. Voinov (1973)

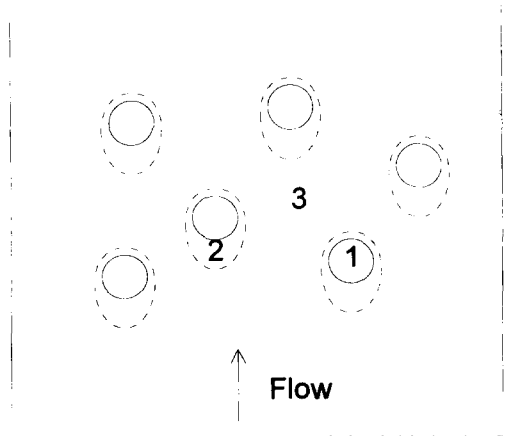

Figure 1. Schematic representation of the fields in the flow.

calculated the potential flow around a sphere of radius a. By integrating the pressure forces around the surface of the sphere, the interfacial force $\mathbf{F}_I$ was found to be:

$$\mathbf{F}_I = \frac{4\pi a^3}{3}\rho_L\left[\frac{D\mathbf{u}_0}{Dt} + \frac{1}{2}\left(\frac{D\mathbf{u}_0}{Dt} - \frac{d\mathbf{v}}{dt}\right) + \frac{1}{2}\frac{\dot{a}^3}{a^3}(\mathbf{u}_0 - \mathbf{v}) - \boldsymbol{g}\right] \quad [8]$$

where

$$\frac{D}{Dt} \equiv \frac{\partial}{\partial t} + \mathbf{u}_0 \cdot \nabla \quad [9]$$

$$\mathbf{u}_0 \equiv \nabla\Phi_0, \quad [10]$$

Φ_0 being the potential for flow without bubbles. The velocity $\mathbf{u}_0$ corresponds to the interstitial velocity. Lhuillier (1982) also used potential theory and found the same expression for this force.

Thomas *et al.* (1983) assumed that we can simply add a lift force $\mathbf{F}_L$ when the sphere is in a rotational straining flow, and a drag force $\mathbf{F}_D$ to take into account liquid viscosity, or:

$$\mathbf{F}_L = -\rho_L \frac{4\pi a^3}{3} C_L(\mathbf{v} - \mathbf{u}_0) \times \mathbf{w} \quad [11]$$

where C_L is a lift coefficient,

$$\mathbf{w} = \nabla \times \mathbf{u}_0 \quad [12]$$

and

$$\mathbf{F}_D = -\rho_L \frac{4\pi a^3}{3} \frac{|\rho_p - \rho_L|}{\rho_L} \boldsymbol{g} \frac{(\mathbf{v} - \mathbf{u}_0)}{V_t} f\left(\frac{|\mathbf{v} - \mathbf{u}_0|}{V_t}\right) \quad [13]$$

where $f \equiv 1$ when the liquid is pure and $f \equiv |\mathbf{v} - \mathbf{u}_0|/V_t$ when the bubble is in a contaminated liquid; ρ_p is the inclusion density and V_t the rise velocity.

The momentum balance then becomes:

$$\mathbf{F} = \mathbf{F}_I + \mathbf{F}_L + \mathbf{F}_D = \rho_P \frac{4\pi a^3}{3}\left(\frac{d\mathbf{v}}{dt} - \boldsymbol{g}\right). \quad [14]$$

A numerical simulation conducted by Rivero (1991) on the separation of the different forces appearing in the total force on a spherical inclusion, showed that in a steady and spatially accelerated flow, the inertial term is $D\mathbf{u}_0/Dt + C_m(D\mathbf{u}_0/Dt - d\mathbf{v}/dt)$, where $C_m = 1/2$ even for viscous fluid ($Re < 300$). This result justifies the fact that we can, therefore, directly add a viscous drag term to the inertial term without changing it. However, the expression of this inertial term deserves some clarification.

In [8] the sum $\rho D\mathbf{u}_0/Dt - \rho\boldsymbol{g}$ is often identified with the action of the pressure force on the dispersed phase and the remaining terms in right side of [8] are then associated with an interfacial force. This decomposition is often the origin of the following modelling error.

If we first consider the case where $\mathbf{u}_0$ is taken as the reference liquid velocity, Couet *et al.* (1991), for instance, write:

$$\rho_L \frac{D\mathbf{u}_0}{Dt} - \rho_L \cdot \boldsymbol{g} = -\nabla P_0 \quad [15]$$

and include the pressure gradient ∇P_0 in the total force exerted on an inclusion. The problem comes from [15] which can be read as a liquid momentum balance. This equation is still correct when there is only a single bubble in the flow, but is not rigorously verified when the void fraction increases. As it will be shown in section 3.2, the momentum balance for the continuous liquid is different from [15]. It is so proper to keep [8] in its original form, since $\mathbf{u}_0$ varies with the void fraction, as expressed by the liquid momentum balance.

Secondly, if we consider the case where the mean velocity u is taken as the reference liquid velocity, it is often written that:

$$\rho_L \frac{Du}{Dt} - \rho_L \cdot \boldsymbol{g} = -\nabla P \quad [16]$$

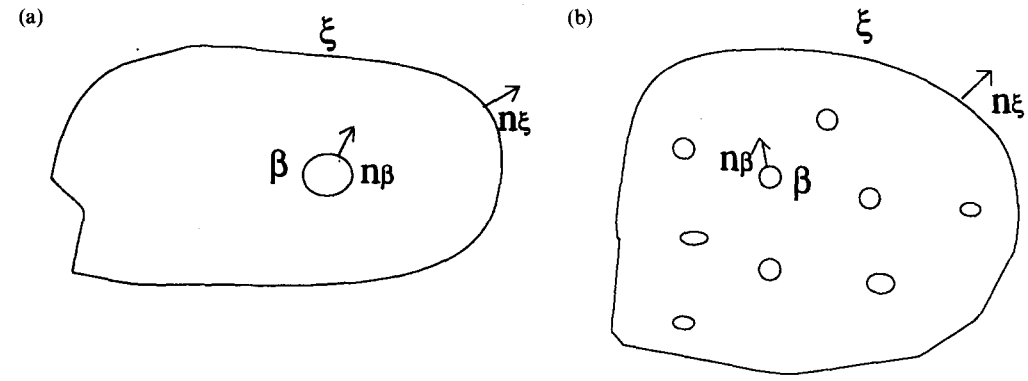

Figure 2. Boundary surfaces used to express the liquid momentum balance (a) when only one bubble is considered; (b) when several bubbles are considered.

and the pressure gradient is incorporated in the force exerted on the inclusion. The left side of [16] is only due to liquid acceleration and is included in the interfacial force between the liquid and the bubble, therefore, it must not interfere in the mixture momentum balance. By splitting the total force exerted on the inclusion into a pressure gradient force and an interfacial force (an added mass force and a viscous drag force), this pressure gradient is typically included in the mixture momentum, thus being considered twice.

Following this line of reasoning for the interfacial force, the liquid momentum balance should be written as:

$$\rho_L \frac{\mathbf{Du}}{\mathbf{D}t} = -\nabla P + \rho_L \mathbf{g} - \frac{\epsilon}{1-\epsilon}\rho_L C_m\left(\frac{\mathbf{Du}}{\mathbf{D}t} - \frac{\mathbf{dv}}{\mathrm{d}t}\right) + \frac{\epsilon}{1-\epsilon}|\rho_L - \rho_p|\mathbf{g}\frac{(\mathbf{v}-\mathbf{u})}{V_t} f\left(\frac{|\mathbf{v}-\mathbf{u}|}{V_t}\right). \quad [17]$$

Equation [17] is clearly in contradiction with [16] when the void fraction has a finite value: here also it is better to keep the inertial terms in their original form.

3.2. *Momentum equation for the continuous phase*

By writing a momentum balance for the continuous liquid phase occupying the volume V_L, included between the surface β delimiting the bubble and a bounding surface ξ (figure 2(a)), we obtain, after projection on the i-axis, an equation similar to [13] of Kowe *et al.* (1988):

$$\int_\xi \left(pn_i + \rho_L u_i u_j n_j - \eta \frac{\partial u_i}{\partial t} n_j\right) \mathrm{d}S = -\rho_L \int_{V_L} \left(\frac{\partial u_i}{\partial t} - \frac{\partial u_{0i}}{\partial t}\right) \mathrm{d}V$$

$$- \int_{V_L} \rho_L \left(\frac{\partial u_{0i}}{\partial t} - g_i\right) \mathrm{d}V + \int_{V_L} \left(-pn_i + \eta \frac{\partial u_i}{\partial x_j} n_j\right) \mathrm{d}S + \int_\beta \rho_L u_i u_j n_j \mathrm{d}S \quad [18]$$

where u_i is the liquid velocity irrespective of whether we are, near or far from the bubble ($V_L > C_m V_b$).

Kowe *et al.* (1988) have proposed several transformations of the right side of [18]. Here we propose a slightly different derivation of the last term.

Assuming that there is no mass transfer between the phases we can write:

$$\int_\beta u_i u_j n_j \mathrm{d}S = v_j \int_\beta u_i n_j \mathrm{d}S \quad [19]$$

since

$$u_j n_j = v_j n_j \quad [20]$$

and assuming that the inclusions are small symmetrical particles in an inviscid straining flow, Kowe *et al.* (1988) write that:

$$v_j \int_\beta u_i n_j \mathrm{d}S = V_b v_j \frac{\partial u_{0i}}{\partial x_j}. \quad [21]$$

No more details are provided by these authors. This equation can, however, be derived from Voinov's potential Φ by expressing it in terms of spherical harmonics and taking into account the orthogonal properties of these harmonics over a sphere. Kowe *et al.* (1988) mention a problem with this term when they compared their computational results with the experimental data of Lewis & Davidson (1985), and proposed to suppress it, as it should be the case with solid particles.

In a first step, we have determined the weight of this term by analysing the Kowe *et al.* (1988) predictions with experimental data not used by these authors.

In determining discharge coefficients of standard nozzles for single and two-phase flows, Doroshenko (1974) measured the pressure drop through nozzles with void fractions of 10, 20, 30 and 40%. The two phase flows are homogenized by the diverting part of a mixing device situated upstream of the tested nozzle. Standard nozzles (figure 3(a)) with different area ratios were used and inserted in a horizontal pipe with an internal diameter of 98 mm.

We have computed the pressure drop for the nozzle of figure 4 with an area ratio of 0.21 and a void fraction of 30%, using [20b] presented by Kowe *et al.* (1988) and the same equation without $-v\partial u_0/\partial x$ (a full discussion of these data will provided in section 5). We can clearly see on figure 4 a large discrepancy between the numerical results when the term $-v\partial u_0/\partial x$ is used, and the experimental data for a wide range of liquid velocities. This effect has been mentioned by Kowe *et al.* (1988) for liquid velocities less than 0.1 m/s in vertical flows. Figure 4 shows that this trend is still present with higher values of the liquid velocity (up to 3 m/s) in horizontal flows. The Kowe

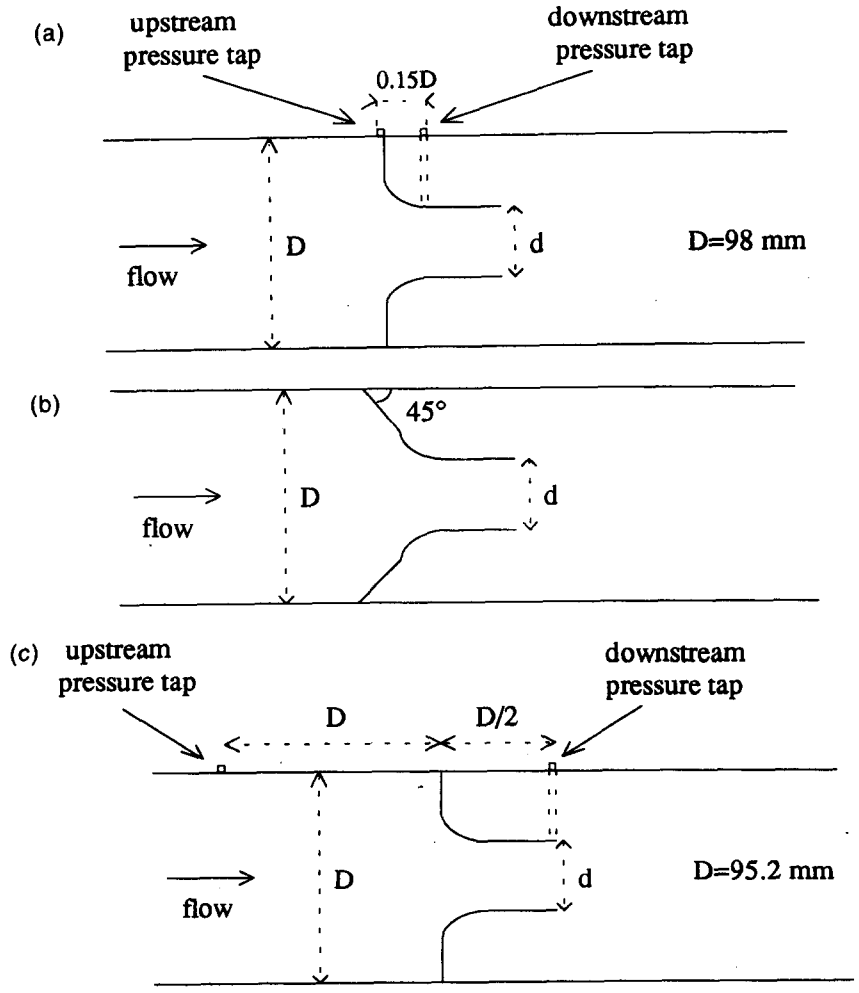

Figure 3. (a) Nozzle used by Dorshenko (1974); (b) Nozzle used for numerical resolution; (c) Nozzle used by Lewis & Davidson (1985).

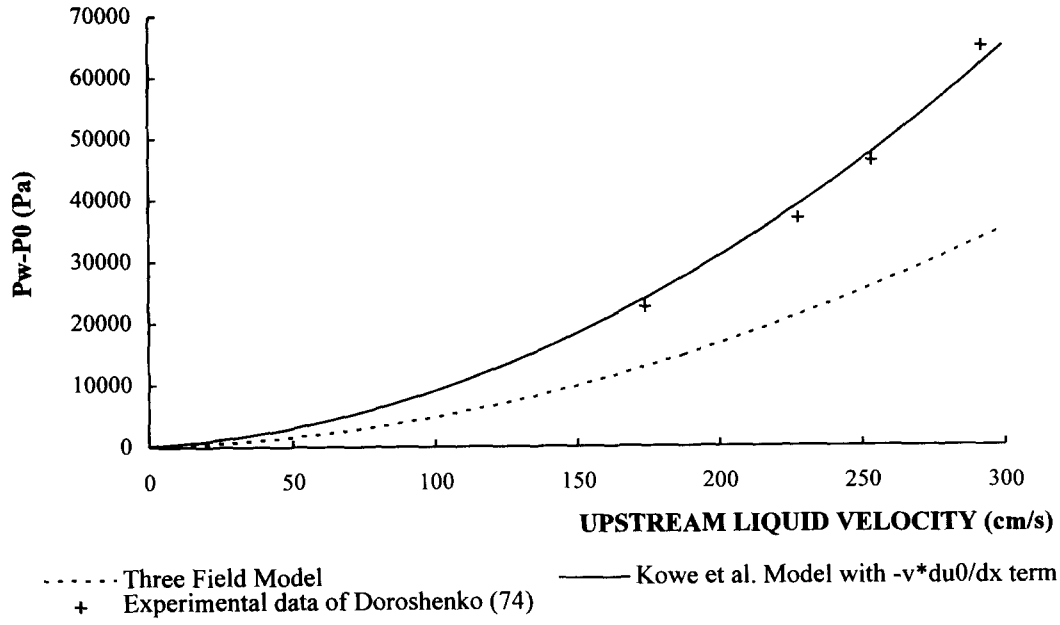

Figure 4. Comparison between the three-field model and the Kowe *et al.* model when $-v\,du_0/dx$ term is remained with experimental data of Doroshenko (1974) for an upstream void fraction of 30% and a throat diameter of 4.5 cm.

et al. (1988) model underpredicts the pressure drop with an error of about 35%. These results show that there are reasons to suspect the derivation of [21].

The problem arises, according to us, from the potential flow theory assumption. This expression would be valid if the entire external flow was fully potential. However, the velocity derivatives in that case would not satisfy the tangential stress boundary condition. Thus, a boundary layer still exists on the bubble surface. The boundary layer is much thinner and remains attached to the surface longer than on a comparable rigid body, but it implies a velocity variation across itself and a continuity of the tangential velocities, so we should have written:

$$u_i n_j = v_i n_j. \qquad [22]$$

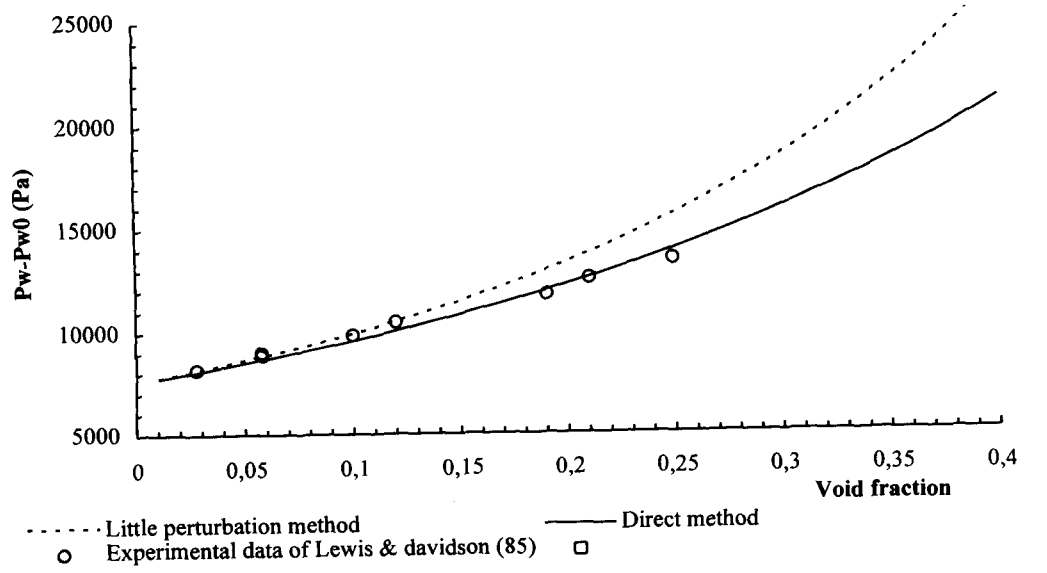

Figure 5. Comparison between numerical resolution by the direct method and the little perturbations method with experimental data of Lewis & Davidson (1985) when the liquid superficial velocity is 65 cm/s and the throat diameter is 4 cm.

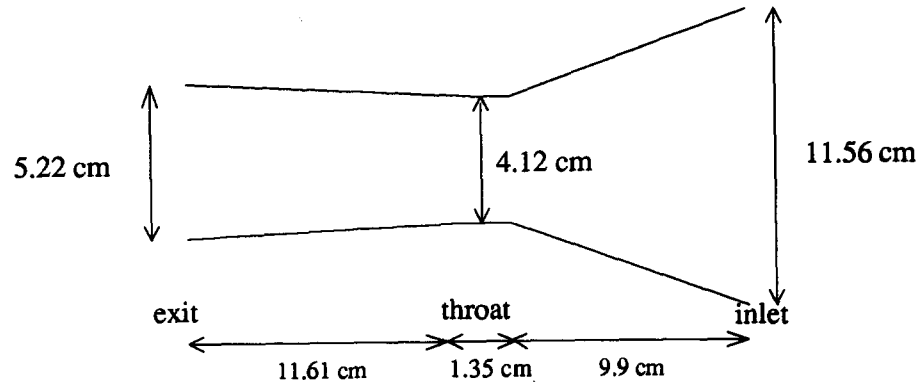

Figure 6. Venturi used by Kuo & Wallis (1988). Inlet cross section area = 59.47 cm^2, throat to inlet cross section area ratio = 0.36, outlet to inlet cross section area ratio = 0.452.

If the particles are small enough so that the flow around them is axisymmetrical, say in relation to the i-axis, the internal flow in the particle will also become symmetrical with regard to this axis, and so we can write:

$$\int_{V_b} \frac{\partial v_i}{\partial x_j} \mathrm{d}S = 0 \quad \text{for } j \neq i \qquad [23]$$

since

$$\frac{\partial}{\partial x_j} = 0 \quad \text{for } j \neq i. \qquad [24]$$

To express the last integral we have written a mass balance for the particle:

$$\int_{V_b} \frac{\partial v_i}{\partial x_i} \mathrm{d}V = -\int_{V_b} \sum_{i \neq j} \frac{\partial v_i}{\partial x_j} \mathrm{d}V = 0 \qquad [25]$$

and finally obtained that:

$$v_j \int_\beta v_i n_j \mathrm{d}S = v_j \int_{V_b} \frac{\partial v_i}{\partial x_j} \mathrm{d}V = 0. \qquad [26]$$

This result is quite consistent with the three-field flow assumption that defines a volume of liquid attached to the bubble flowing with the same velocity.

The momentum balance when there is only one bubble is written as:

$$\int_\xi \left(p n_i + \rho_L u_i u_j n_j - \eta \frac{\partial u_i}{\partial x_j} n_j \right) \mathrm{d}S = -\rho_L \int_V \left(\frac{\partial u_{0i}}{\partial t} - g_i \right) \mathrm{d}V - F_i - \rho_L V_b \left[C_m \left(\frac{\mathrm{d}v_i}{\mathrm{d}t} - \frac{\partial u_{0i}}{\partial t} \right) + g_i \right]. \qquad [27]$$

Now considering that the control surface ξ contains N inclusions of arbitrary size, we obtain a momentum balance quite similar to [21] of Kowe *et al.* (1988):

$$\int_\xi \left(p_0 n_i + \rho_L u_{0i} u_{0i} n_j \right) \mathrm{d}S + \int_\xi \delta M_1 = -\rho_L \int_V \left(\frac{\partial u_{0i}}{\mathrm{d}t} - g_i \right) \mathrm{d}V - \sum_{i=1}^{N} \left[F_i^{(n)} - V^{(n)} \rho_L \left\{ C_m \left(\frac{\mathrm{d}v_i}{\mathrm{d}t} - \frac{\partial u_{0i}}{\partial t} \right) + g_i \right\} \right] \qquad [28]$$

where

$$\delta M_1 = \int_\xi \left[(\langle P \rangle - P_0) n_i + \rho_L (\langle u_i u_j \rangle - u_{0i} u_{0j}) n_j - \eta \frac{\partial u_{0i}}{\partial x_j} n_j \right] \mathrm{d}S. \qquad [29]$$

$\langle\rangle$ represents a volume average within the liquid alone and η is the liquid dynamic viscosity. We need to evaluate the differences between $\langle P \rangle$ and P_0 and between $\langle u_i u_j \rangle$ and $u_{0i} u_{0j}$ which are caused

by additional kinetic energy and momentum flux in the liquid near the bubbles. Using, as Kowe *et al.*, potential theory but remaining consistent with Voinov's calculations we find slightly different results:

$$\langle P\rangle - P_0 = -\rho_L \frac{\epsilon}{1-\epsilon}\left[\frac{1}{2}C_m(v_i-u_{0i})(v_i-u_{0i}) + \frac{a^2}{15}\frac{\partial u_{0i}}{\partial x_j}\frac{\partial u_{0i}}{\partial x_j}\right]. \quad [30]$$

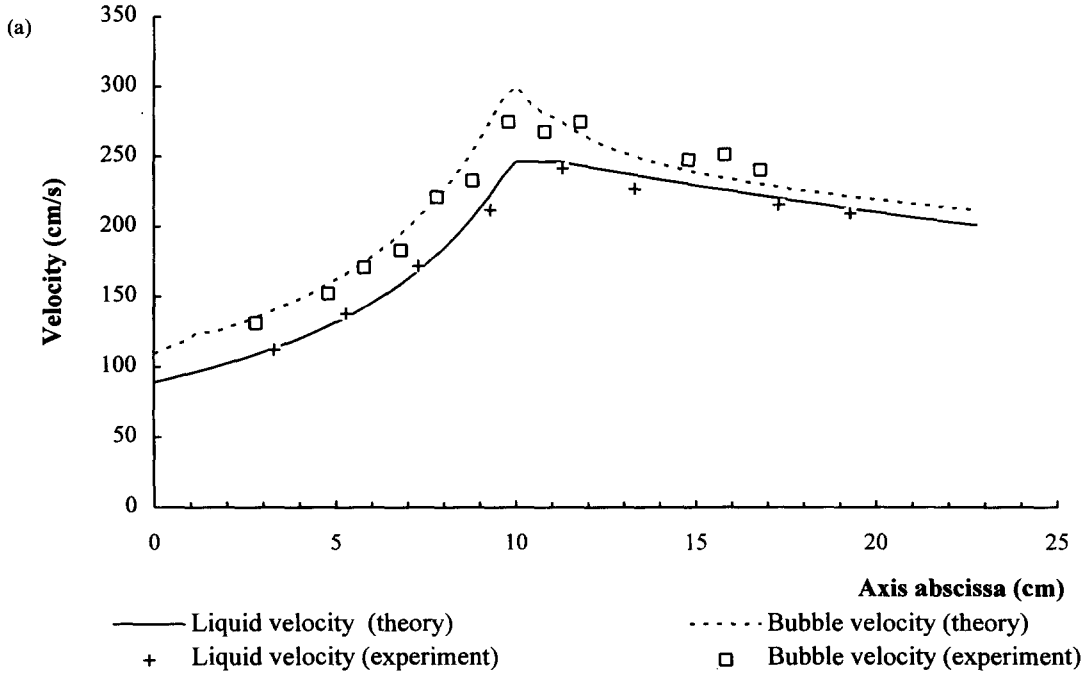

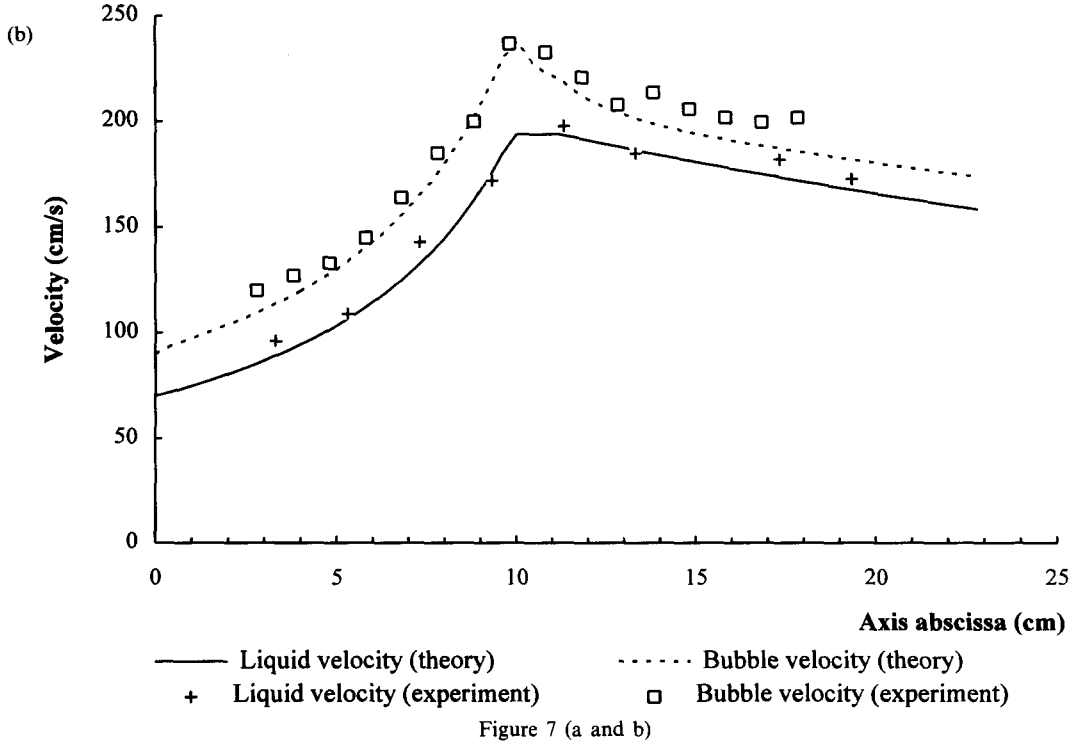

Figure 7 (a and b)

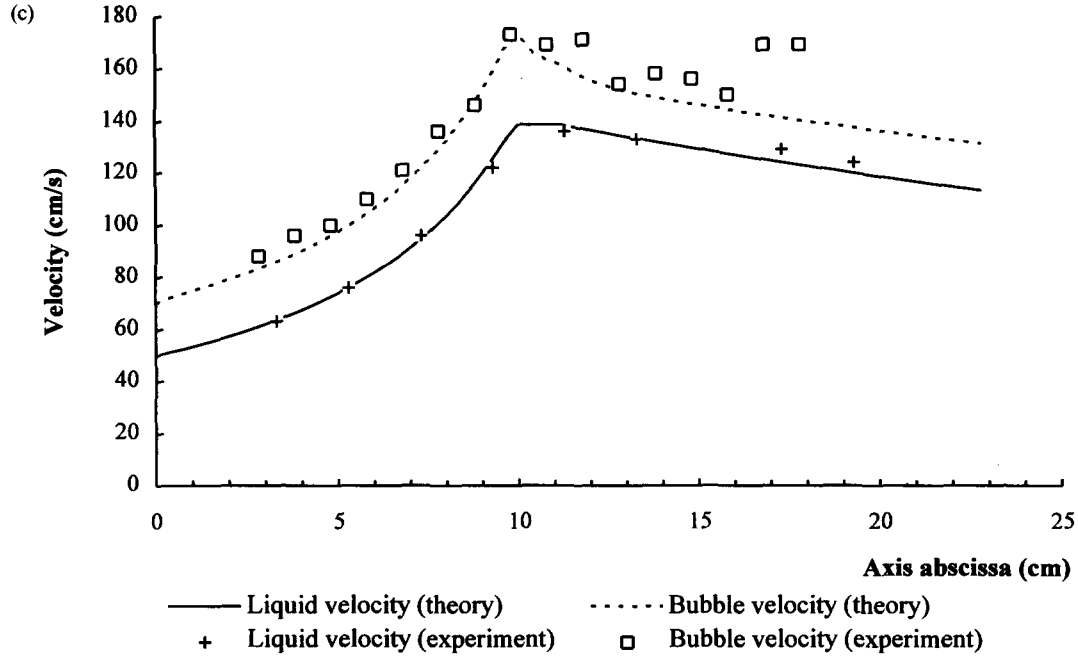

Figure 7. Comparison between calculated velocities with the three-field model and measured ones obtained by Kuo & Wallis (1988) when the upstream liquid velocity is (a) 50 cm/s; (b) 70 cm/s; (c) 89 cm/s.

To express $\langle u_i u_j \rangle - u_{0i} u_{0j}$ we do not use only diagonal terms (as did Kowe *et al.*) but also include the i, j terms:

$$\langle u_i u_j \rangle - u_{0i} u_{0j} = \rho_L \frac{\epsilon}{1-\epsilon} \left[\frac{1}{20} (v_i - u_{0i})(v_j - u_{0j}) + \frac{3}{20} \delta_{ij} (v_i - u_{0i})(v_i - u_{0i}) + \frac{4}{105} a^2 \frac{\partial u_{0i}}{\partial x_k} \frac{\partial u_{0j}}{\partial x_k} + \frac{2}{63} a^2 \delta_{ij} \frac{\partial^2 u_{0i}}{\partial x_k \partial x_k} \right]. \quad [31]$$

Equations [30] and [31] show extra terms when compared to the Kowe *et al.* (1988) expressions. These terms take into account the unsymmetric distribution of kinetic energy and momentum flux around the particle. These new terms are scaled by the ratio of the bubble diameter to the flow length scale $(a/L)^2$. These may be small, however in the case of rapid contraction and very low velocity slip, they may remain of the same order of magnitude as the main terms $(v_i - u_{0i})(v_j - u_{0j})$ and must not be neglected.

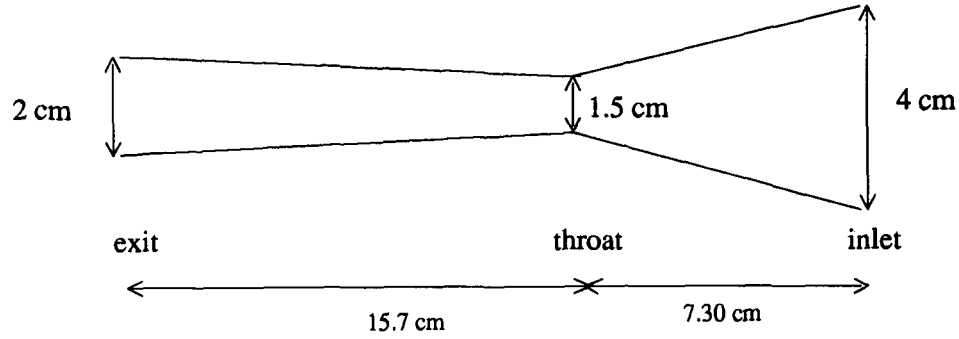

Figure 8. Two dimensional nozzle used by Ishii *et al.* (1992). Inlet cross section area = 6 cm^2, throat to inlet cross section area ratio = 0.5, outlet to inlet cross section area = 0.375.

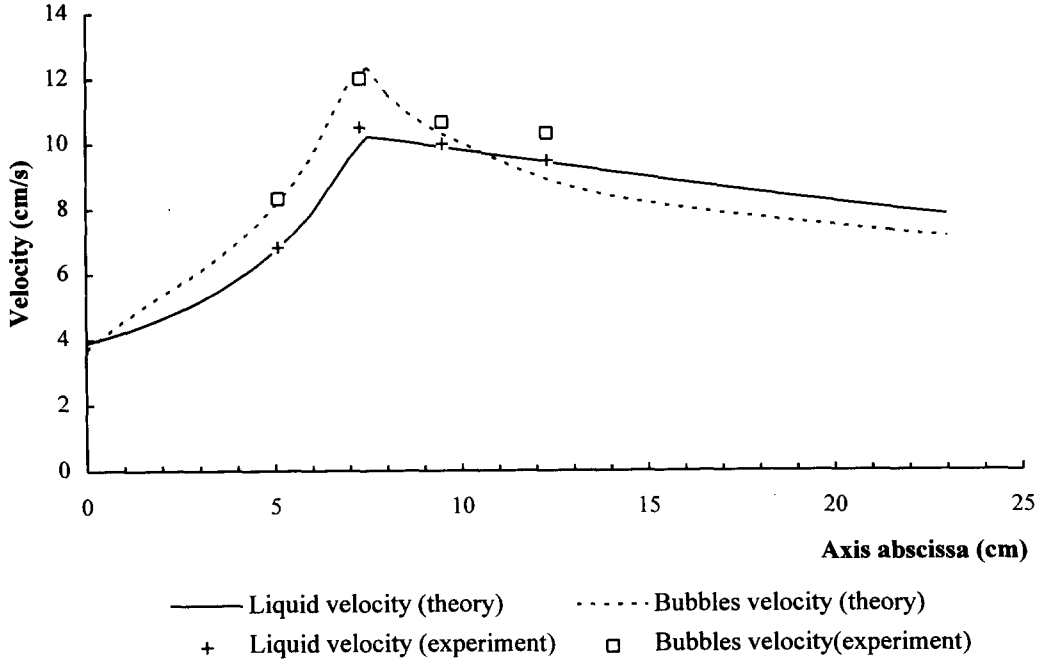

Figure 9. Comparison between calculated velocities with the three-field model and measured ones obtained by Ishii *et al.* (1992) when the upstream liquid velocity is 390 cm/s and the void fraction is 5%.

4. NUMERICAL SOLUTION FOR BUBBLE OR DROPLET FLOWS THROUGH A CONTRACTION

In the remaining sections we assume steady state, one dimensional flow through a contraction and that all inclusions have the same diameter. With these assumptions our model can be described by a system of six equations projected on the x-axis of the pipe:

$$\frac{\mathrm{d}}{\mathrm{d}x}\{[u_0(1-\epsilon)+C_m\epsilon(v-u_0)]A\}=0 \tag{32}$$

$$\frac{\mathrm{d}}{\mathrm{d}x}[\epsilon vA]=0 \tag{33}$$

$$\rho_p\left[v\frac{\mathrm{d}v}{\mathrm{d}x}+g\cos\alpha\right]=\rho_L\left[(1+C_m)u_0\frac{\mathrm{d}u_0}{\mathrm{d}x}-C_m v\frac{\mathrm{d}v}{\mathrm{d}x}+g\cos\alpha-g\frac{(v-u_0)}{V_t}f\left(\frac{|v-u_0|}{V_t}\right)\right]=F \tag{34}$$

$$\frac{\mathrm{d}}{\mathrm{d}x}[A(P_0+\rho_L u_0^2+\delta M)]=P_w\frac{\mathrm{d}A}{\mathrm{d}x}-\tau_w 2\pi R-A[\epsilon F+(1-\epsilon)\rho_L g\cos\alpha] \tag{35}$$

$$\delta M=-\rho_L\frac{\epsilon}{1-\epsilon}\left[\frac{1}{20}(v-u_0)^2\right] \tag{36}$$

$$P_w=P_0-\frac{1}{2}C_m\frac{\epsilon}{1-\epsilon}(v-u_0)^2 \tag{37}$$

where

$$\tau_w=\frac{1}{2}\rho_L f_w u_0^2 \tag{38}$$

$$f_w=0.079\left(\frac{2u_0R\rho_L}{\eta}\right)^{-\frac{1}{4}}. \tag{39}$$

ρ_p is the dispersed phase density, R the pipe radius, and α the inclination angle of the pipe.

Knowing the upstream values of the independent variables, we can calculate the velocities u_0 and v, the void fraction and the pressure P_0 by solving numerically the set [32]–[39]. Then the last variables P_w and $\langle u \rangle$ can be deduced.

To solve an equivalent system when the particles are assumed to be bubbles, Kowe *et al.* (1988) used a first-order perturbation method for the velocities u_0 and v. Using this method, they directly obtained the velocities $u_0^{(0)}$ and $v^{(0)}$ when there is a single bubble in the flow. However, large errors occur in the results when the upstream void fraction is greater than 10%, as shown in figure 5.

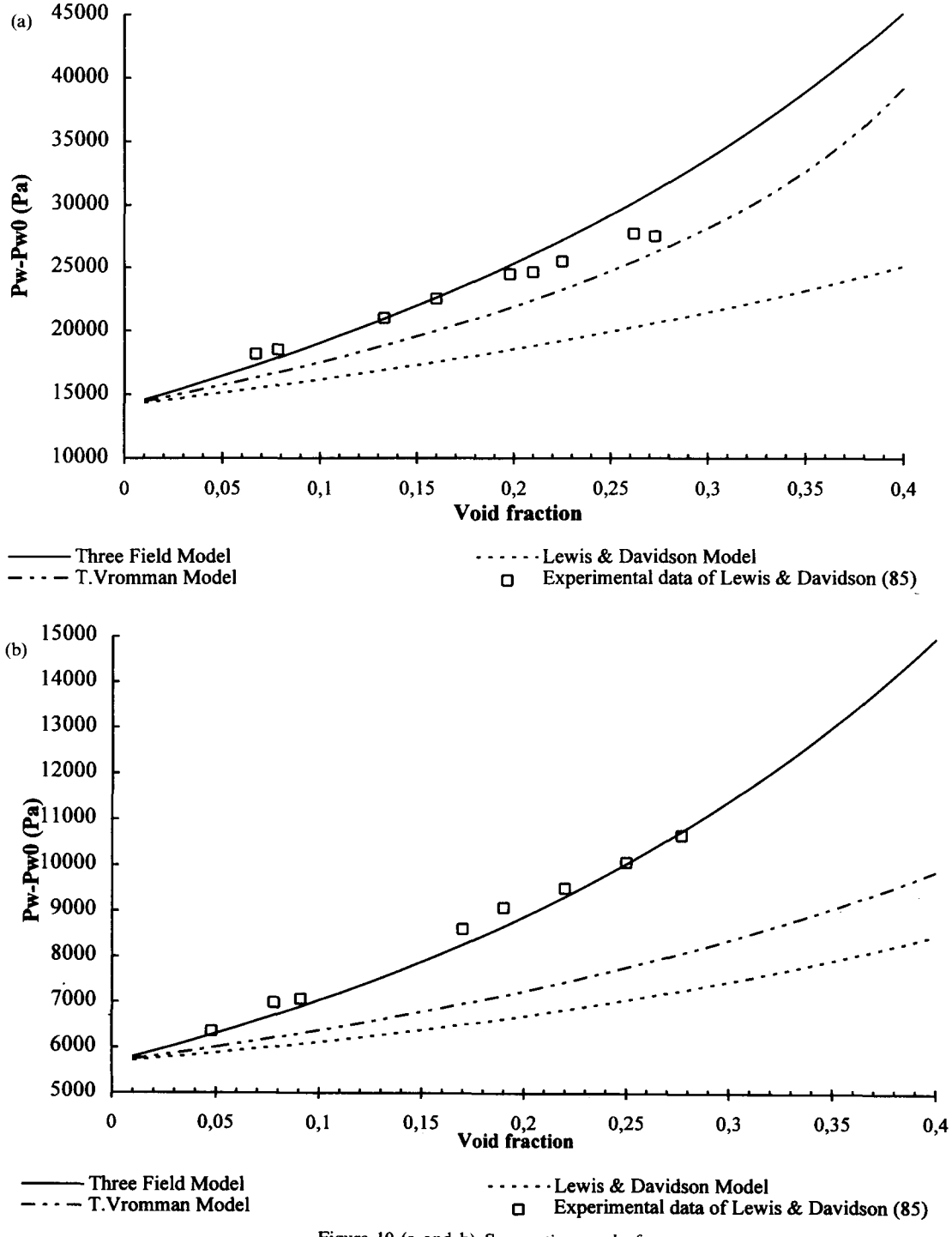

Figure 10 (a and b) *See caption overleaf*

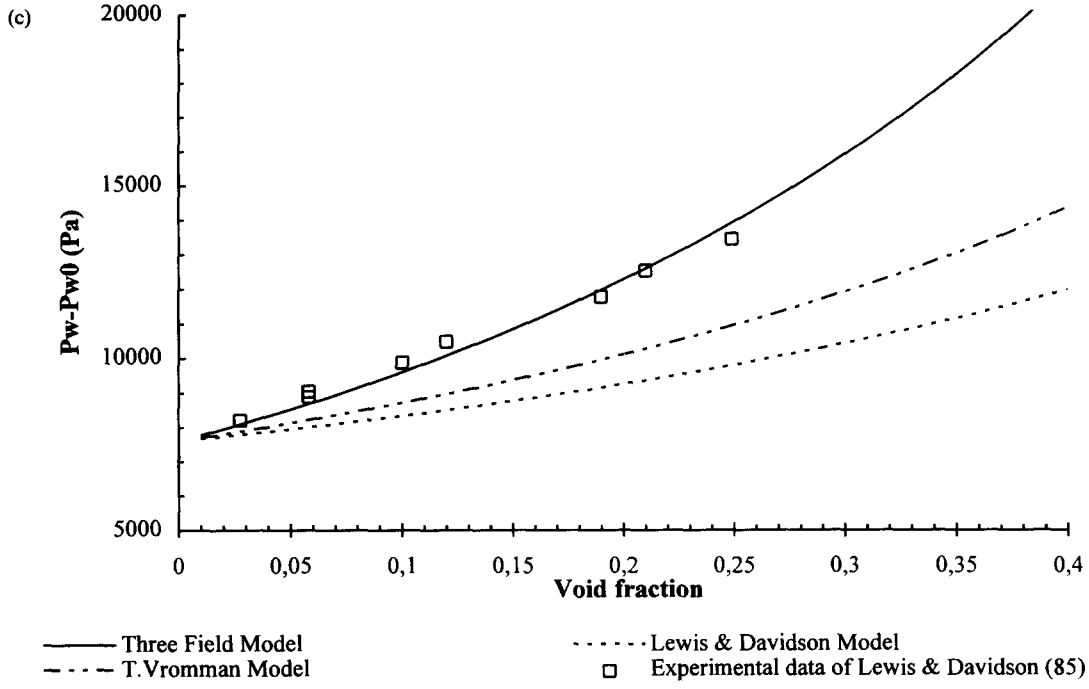

Figure 10. Comparison between theoretical models and experimental data of Lewis & Davidson (1985) when (a) the liquid superficial velocity is 52 cm/s and the throat diameter is 3 cm; (b) the liquid superficial velocity is 54 cm/s and the throat diameter is 4 cm; (c) the liquid superficial velocity is 65 cm/s and the throat diameter is 4 cm.

5. RESULTS

5.1. Velocity profiles

The three-field model (TFM) estimates the influence of phase slip inside the liquid phase, therefore, it was natural to assess the prediction of the difference between particle and liquid velocities.

Among the few experiments available, Kuo & Wallis (1988) measured the bubble and the liquid velocities in an upward flow through a Venturi (figure 6). Eighteen rows of phototransistors were placed along the Venturi, spaced on 1 cm intervals, to track the bubble trajectory and determine its velocity. The liquid velocity was measured using a Pitot tube.

Figure 7(a)–(c) shows a comparison between numerical results obtained from the three-field model and the experimental data of Kuo & Wallis (1988). The bubble deviating little from the Venturi axis during its motion, the upstream liquid velocity used in the calculations is the velocity measured on the Venturi axis upstream of the convergent. The function used for viscous drag was $f \equiv |v - u|/V_t$ with $V_t = 20$ cm/s (this value having been measured by Kuo & Wallis 1988).

For upstream liquid velocities of 50 and 70 cm/s (figure 7(a) and (b)) the model predicts the velocity slip along the convergent section and the throat entrance quite well. In the divergent portion, the bubble velocity values flatten and deviate from the numerical results. After the throat, the effect of turbulence increases significantly and the lift forces drive the bubble out of its rectilinear trajectory and create strong velocity fluctuations.

For the upstream liquid velocity $u_0(0) = 89$ cm/s, the numerical results deviate from the experimental data, as the bubble velocity is overestimated by the TFM, and the viscous drag seems to be too weak. Indeed, the bubble diameter is reported to vary in these experiments between 1.5 and 2 mm, and the greater the liquid flow rate, the smaller the bubble diameter. For $u_0(0) = 89$ cm/s, this diameter is probably closer to 1.5 mm. If we use [7.9] found in Clift *et al.* (1978) to calculate the rise velocity, we find $V_t = 16$ cm/s for $d_b = 1.5$ mm instead of 20 cm/s for $d_b = 2$ mm. This new value produces better agreement between numerical results and experimental data. This shows the

importance of correctly modelling the rise velocity as a function of bubble diameter, and the necessity of determining the bubble size.

More recently Ishii *et al.* (1992) conducted velocity measurements of liquid and bubbles in bubbly flows through a Venturi for the case of non vanishing void fraction, and for much greater liquid velocities than in the Kuo & Wallis experiments. They utilised a vertical downward flow through a two-dimensional nozzle, with dimensions presented in figure 8. The upstream void fraction, liquid

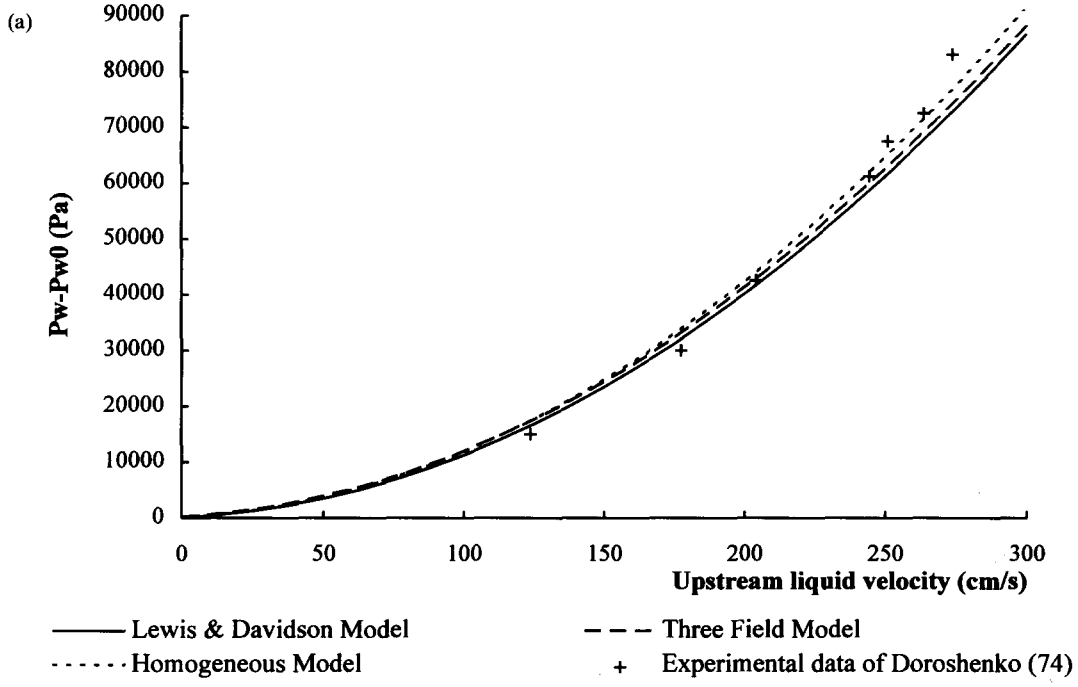

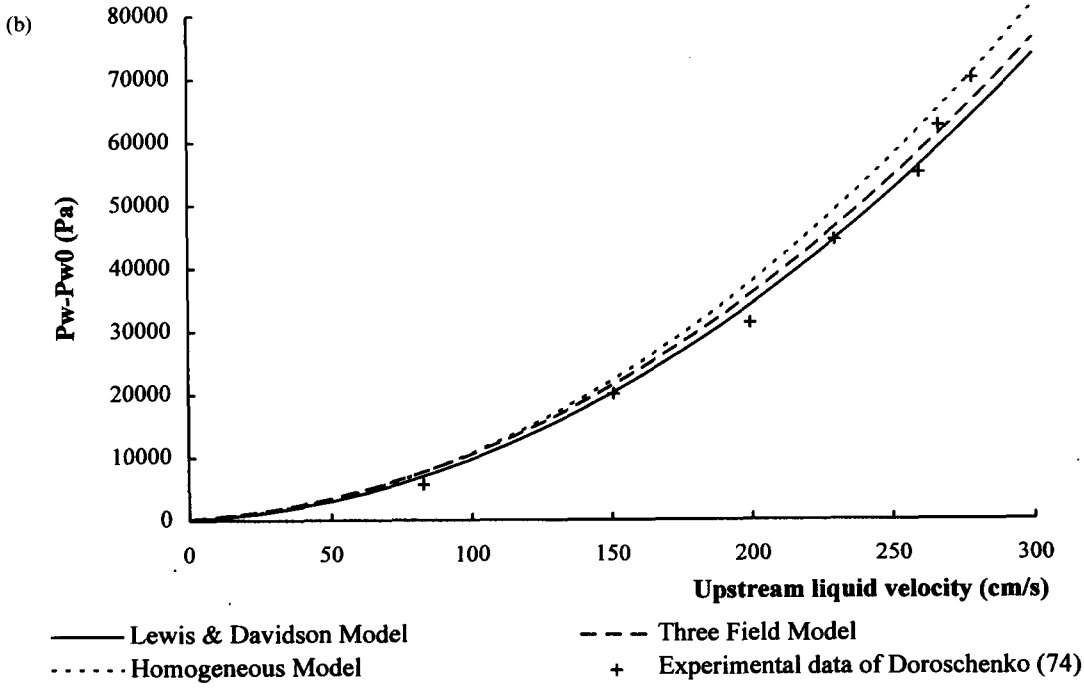

Figure 11 (a and b) *See caption overleaf*

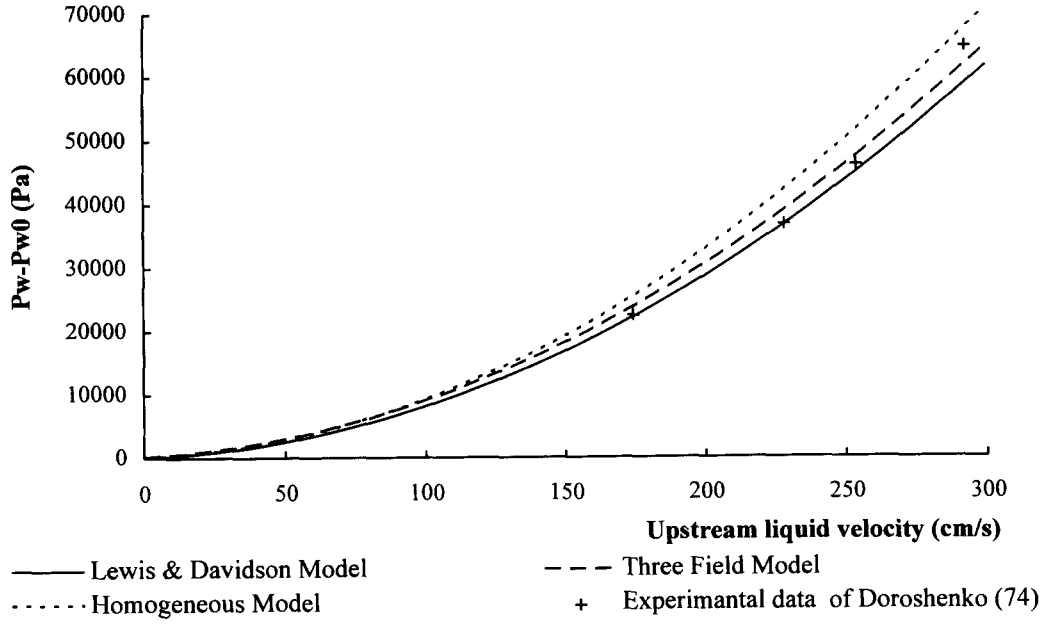

Figure 11. Comparison between the theoretical models and experimental data of Doroshenko (1974) when the upstream void fraction is (a) 10%; (b) 20%; (c) 30%.

velocity and pressure were, respectively, 5%, 3.9 m/s and 1.8 bar. The bubble velocities were measured using double exposure photographs separated by several hundred microseconds.

It can be surprising to see on figure 9 that, in the diverging part of the Venturi, the theoretical bubble velocity becomes smaller than the liquid velocity. In fact, the flow being downward, when the liquid velocity decreases, the buoyancy force opposed to the inertial forces comes strong enough to impose an equilibrium bubble velocity smaller than the liquid velocity. No turbulent forces being incorporated in the model, it is less able to predict correctly the measured velocity in the diverging part. Nevertheless, figure 9 shows that the TFM is quite able to predict the velocity slip between bubbles and liquid at a moderate value of the void fraction.

5.2. Pressure drops—comparison with classical models

We have first compared the TFM predictions with the experimental data of Lewis & Davidson (1985), who measured pressure drops across a standard nozzle with upward vertical bubbly flows. These bubbly flows are homogenised with two successive perforated plates upstream of the different nozzles used. Nozzle geometry and pressure tap locations are described on figure 3(c).

As the cross-sectional area gradient is infinite at the nozzle entrance, we use an equivalent nozzle shape (figure 3(b)) when computing pressure drops.

Figure 10(a)–(c) presents the calculated pressure drop, including the water column weight $\epsilon\rho_L gH$ (where H is the distance between pressure taps) consistently with the procedure used by Lewis & Davidson, as a function of the upstream void fraction for specified liquid superficial velocities of 54 and 65 cm/s and throat diameters of 3 and 4 cm. The numerical results obtained with the TFM, the LDM and that of Vromman (1988) are presented.

For liquid superficial velocities of 54 and 65 cm/s, the TFM model results are quite good, as it predicts the pressure drop within 4% of the experimental data, for all values of the void fraction. For $U_{LS} = 52$ cm/s and a throat diameter of 3 cm, the error is less than 5% for void fractions less than 25%. In comparison, the two-fluid models deviate significantly from the experimental data and result in errors of approximately 20% for Vromman's model and 30% for the LDM.

Figure 11(a)–(c) shows similar comparisons with the experimental data of Doroshenko (1974). As the two-fluid model of Vromman (1988) gives in this case, results very close to those of the LDM, we have used the HM as a third model for comparison. Doroshenko set pressure taps as recommend the standard ISO 1932, thus we used the correlations proposed by these standards and used a two-phase density ρ instead of the liquid density ρ_L, to compute the pressure drop in

HM. As no details were given by Doroshenko on bubble size, we assumed that the rise velocity was 25 cm/s.

We can see that the HM produces good results for the void fraction presented. For upstream void fractions of 10 and 20%, the close agreement of the three models do not allow us to determine which is better. For the void fraction of 30%, differences in the results increase: the HM tends to overestimate the experimental data, the LDM to underestimate the data, and the TFM provides excellent agreement with the data.

The differences between the models are less pronounced than for the Lewis & Davidson experiments, since the distance over which we integrated the pressure is much smaller—approximately five times. Small differences between the LDM, TFM and HM equations added at every step have a much lower impact on the results.

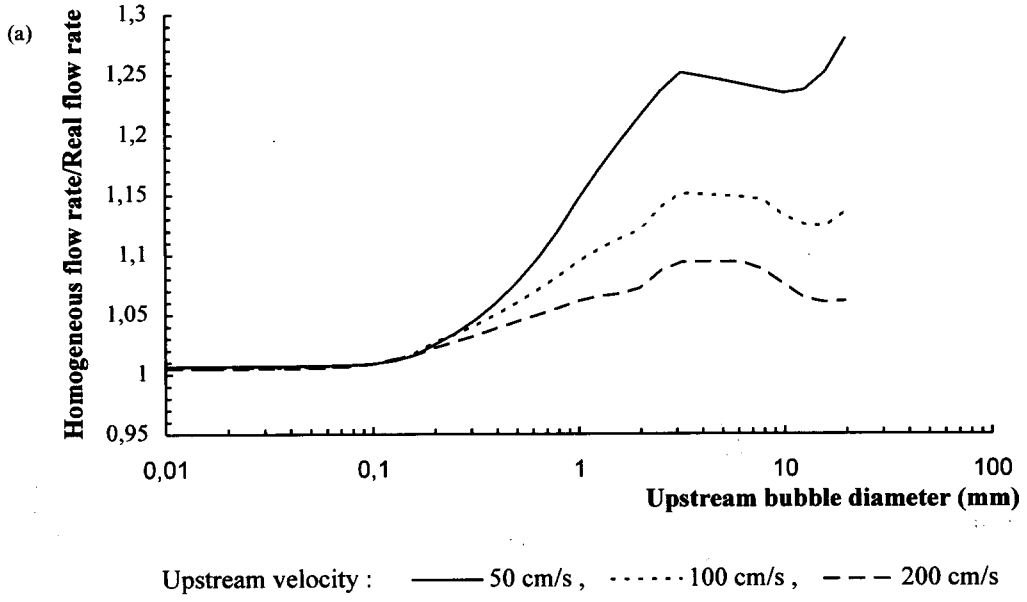

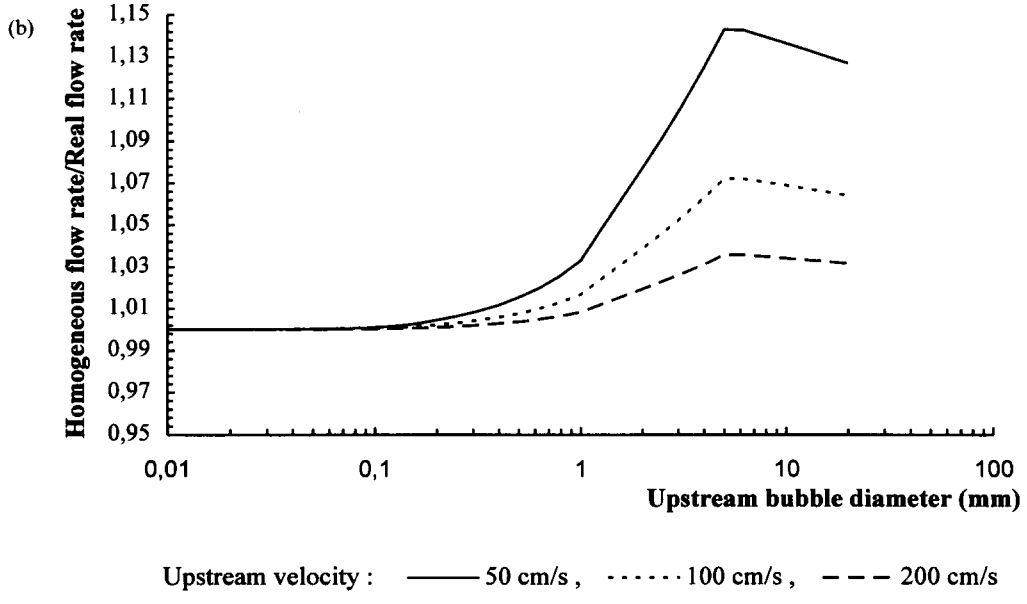

Figure 12 (a and b) *See caption overleaf*

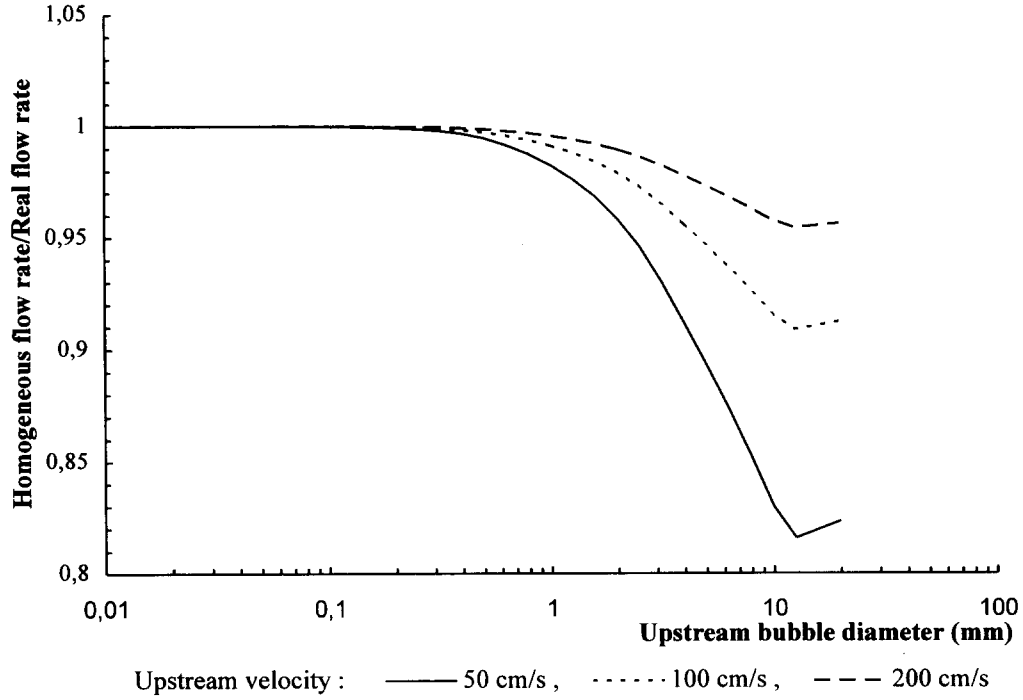

Figure 12. Ratio of the homogeneous flow rate to the real flow rate against bubble diameter for an air/water flow in a Venturi for a void fraction of 30% and a throat to diameter area ratio of 0.1; (b) Ratio of the homogeneous flow rate to the real flow rate against bubble diameter for an oil/water flow in a Venturi for a fraction of oil of 30% and a throat to diameter area ratio of 0.1; (c) Ratio of the homogeneous flow rate to the real flow rate against bubble diameter for an oil/water flow in a Venturi for a fraction of oil of 30% and a throat to diameter area ratio of 0.1.

This comparison performed for two ranges of flow rates and for two pipe inclinations (figures 10 and 11) shows the benefits of the TFM, which are more visible when the distance between pressure taps is increased. Such a comparison should be extended to wider ranges of velocities and to other dispersed flows to further verify its validity, but shows quite positive results for the three-field model, over the more widely known two-fluid models. For this reason we have chosen the TFM to study the influence of bubble or droplet size on the pressure drop through a Venturi, and then its influence on the total mass flow rate evaluation.

5.3. Influence of bubble size on pressure drop

Lastly it was important to study the sensitivity of the TFM to the rise velocity V_t and to the bubble diameter d_b. This allows determination of the ranges of admissible bubble diameters for which the HM still gives good results for pressure drops and, thus, for mean velocities.

The correlations for V_t proposed by Clift *et al.* (1978) were chosen. We used (3-18) (Clift *et al.* 1978) for spherical bubbles, when d_b is less than 1 mm, (7-5) to (7-9) (Clift *et al.* 1978) for ellipsoidal bubbles when d_b is between 1 and 18 mm, and (8-5) and (8-11) (Clift *et al.* 1978) for large deformed fluid particles when d_b is greater.

To estimate the influence of the bubble diameter on the flow rate measurements, first, the pressure drop across a linear contraction (designed according to the French standard NF X 10-102), in a vertical pipe has been calculated by the TFM. For each value of pressure drop we calculated the flow rate Q_H we would have found from the homogeneous model. The results are presented as the ratio of the volumetric flow-rate Q_H to the real flow rate Q_R (i.e. Q_H/Q_R). The convergent length is 10 cm, the throat area to pipe ratio is 0.1, and the pressure taps are located at the convergent entrance and 15 cm downstream of this location. Three types of upward flows were investigated: a bubbly air–water flow, an oil–water flow with, water as the continuous phase, and a water–oil flow with oil as the continuous phase. The dispersed phase occupied 30% of the entire volume in the three flows.

We can see in figure 12 that, for very small bubble diameters, the flow rate is equal to the flow rate we would obtain with the homogeneous model, as the bubbles are small enough so that there is no slip between phases. When the bubble size increases, the pressure drop increases up to a point where it remains nearly constant, as does the flow rate Q_H.

The lower the real flow rate, the larger the errors that result from the use of the homogeneous model. When the bubble size increases, the HM overestimates the true flow rate by 30% for air–water flows and by about 15% for oil–water flows at the lowest flow rates.

Using these figures, for a given accuracy of the flow rate measurement, we can easily determine the bubble diameter range for which the homogeneous model is valid. If we consider an accuracy of 1%, for air–water bubbly flows the maximum diameter is 130 μm, while for dispersed oil/water flows, diameters up to 300 μm (oil in water droplets) and up to 0.9 mm (water in oil droplets) do not result in deviation stronger than 1% from the homogeneous flow rate.

In figure 12(b) and (c), the oil viscosity was only 10 times greater than the water viscosity. If we increase the oil viscosity to 10^{-4} m^2/s in one case and to 10^{-3} m^2/s in the other case, there is no change for the maximum bubble diameter when the water is the continuous phase, but when the oil is the continuous phase the maximum bubble diameter increases, respectively, to 0.9 and 8 mm.

When we increase the throat to pipe area ratio, the deviation of Q_H is less significant and the maximum bubble diameter for use in the HM increases. This limiting diameter is the input data for the OPTIMIX mixer design procedure and represents what the modelling effort was devoted to.

6. CONCLUSIONS

Even if the hypothesis of dividing the flow into three different fields is still difficult to justify fully, the original approach of Kowe *et al.* has produced very interesting results for the modelling of pressure drops across a convergent section.

The three-field model appears to provide a much better prediction of pressure drops than the classical two-fluid models, where it seems that the primary error results from a wrong interpretation of the interfacial force between the liquid and the bubbles. Further experimental investigations are intended to show its validity in oil–water flows and it has obviously some potential for predicting pressure drops in three-phase air–oil–water flows.

Finally it has been shown that it was possible to determine the critical bubble or droplet diameter beyond which the homogeneous model is no longer valid, for various two-phase flow conditions. In addition, this approach provides the critical bubble or drop diameter that allows us to size the OPTIMIX mixer which is the upstream part of our multiphase flow metering equipment.

REFERENCES

Auton, T. R. 1987 The lift force on a spherical body in a rotational straining flow. *J. Fluid Mech.* **183,** 199–218.

Auton, T. R., Hunt, J. C. R. & Prud'homme, M. 1988 On the motion of cylinders and spheres in inviscid unsteady non uniform rotational flow. *J. Fluid Mech.* **197,** 241–257.

Bataille, J., Lance, M. & Marie, J. L. 1990 Bubbly turbulent shear flows. In *Advance in Gas–Liquid Flows*, FED. Vol. 199. ASME Winter Annual Meeting, November 25–30, Dallas, Texas.

Bensler, H. P. 1990 Détermination de l'aire interfaciale, du taux de vide et du diamètre moyen de Sauter dans un écoulement à bulles à partir de l'atténuation d'un faisceau d'ultrasons. Thèse de doctorat de l'Institut National Polytechnique de Grenoble.

Berne, Ph. 1983 Contribution à la modélisation du taux de production de vapeur par auto-vaporisation dans les écoulements diphasiques en conduite, Thèse de Docteur Ingénieur, Ecole Centrale des Arts et Manufactures, Paris, France.

Biesheuvel, A. & Van Winjgaarden, L. 1984 Two-phase flow equations for a dilute dispersion of gas bubbles in liquid. *Int. J. Multiphase Flow* **10,** 148.

Chislholm, D. 1983 Flow of compressible two-phase mixtures through orifices and nozzles. Heat and Fluid Flow in Nuclear and Process Plant Safety Conference, London.

Couët, B., Brown, P. & Hunt, A. 1991 Two-phase bubbly-droplet flow through a contraction: experiments and a unified model. *Int. J. Multiphase Flow* **17,** 291–301.

Clift, R., Grace, J. R. & Weber, M. E. 1978 *Bubbles, Drops and Particles.* Academic Press, New York.

Cook, T. L. & Harlo F. H. 1984 Virtual mass in multiphase flow. *Int. J. Multiphase Flow* **10,** 691–696.

Darwin, C. 1953 Note on hydrodynamics. *Proc. Camb. Phil. Soc.* **49,** 342–354.

Delhaye, J. M., Giot, M. & Riethmuller, M. L. 1980 *Thermohydraulics of Two-phase Systems for Industrial Design and Nuclear Engineering.* Chap. IV, 72–77. McGraw-Hill, New York.

Delhaye, J. M. 1989 Multiphase flow metering. Int. Multiphase Flow Workshop, Copenhagen.

Doroshenko, V. A. 1974 On the discharge coefficient of nozzles for single and two-phase fluids. *Fluid Mechanics–Soviet Research* **3,** 52–56.

Fairhust, C. P. 1983 BHRA Int. Conf. on the Physical Modelling of Multiphase Flow, Coventry, England, Paper A1.

Hewitt, G. F. 1988 Multiphase mass-flow metering for subsea hydrocarbon production, report produced by IMPEL for the UK Department of Energy.

Hinze, J. O. 1948 Critical speeds and sizes of liquid globules. *Applied Science Research* **A1,** 273–288.

Kowe, R., Hunt, J. C. R., Hunt, A., Couet, B. & Bradburry, L. J. S. 1988 The effects of bubbles on the volume fluxes and pressure gradients in unsteady and non uniform flows of liquids. *Int. J. Multiphase Flow* **14,** 587–606.

Kuo, J. T. & Wallis, G. B. 1988 Flow of bubbles through nozzles. *Int. J. Multiphase Flow* **14,** 547–564.

Ishii, R., Umeda, Y., Murata, S. & Shishido, N. 1993 Bubbly flows through a converging–diverging nozzle. *Phys. Fluids* **A5,** 1630–1643.

Lecoffre, Y., Fournier, F., Lemonnier, H. & Foucrier, M. 1993 Optimix: optimisation, qualification et potentialités d'un mélangeur de conception nouvelle. *Récent Progrès en Génie des Procédés* **7,** 77–85.

Lewis, D. A. & Davidson, J. F. 1985 Pressure drop for bubbly gas-liquid flow through orifice plates and nozzles. *Chem. Eng. Res. Des.* **63,** 149–156.

Lhuillier, D. 1982 Forces d'inertie sur une bulle en expansion se déplaçant dans un fluide. *C. r. Acad. Sci. Paris* **295,** 95–98.

Prosperetti, A. & Jones, A. V. 1984 Pressure forces in disperse two-phase flow. *Int. J. Multiphase Flow* **10,** 425–440.

Rivero, M. 1991 Etude par simulation numérique des forces exercées sur une inclusion sphérique par un écoulement accéléré, Thèse de doctorat, Institut National Polytechnique de Toulouse.

Sevik, M. & Park, S. H. 1973 The splitting of drops and bubbles by turbulent fluid flow. *J. Fluids Engineering* **95,** 53–60.

Thang, N. T. & Davis, M. R. 1979 The structure of bubbly flow through venturis. *Int. J. Multiphase Flow* **5,** 17–37.

Thomas, N. T., Auton, T. R., Sene, K. & Hunt, J. C. R. 1983 Entrapment and transport of bubbles by transient large eddies in multiphase turbulent shear flow, presented at Int. Conf. on the Physical Modelling of Multiphase Flow, Coventry, W. Midlands, Paper E1.

Vromman, T. 1988 Modélisation des écoulements critiques diphasiques dans un homogénéisateur de fluides pétroliers, Thèse de doctorat en Sciences Appliquées de l'Université Catholique de Louvain, Belgique.